Journal of Power Sources 194 (2009) 640–645

Contents lists available at ScienceDirect

Journal of Power Sources

journal homepage: www.elsevier.com/locate/jpowsour

Low-temperature sintering behaviors of nanosized $Ce_{0.8}Gd_{0.2}O_{1.9}$ powder synthesized by co-precipitation combined with supercritical drying

Jinping Liang[a,b], Qingshan Zhu[a,*], Zhaohui Xie[a], Wenlai Huang[a], Chaoquan Hu[a,b]

[a] State Key Laboratory of Multiphase Complex System, Institute of Process Engineering, Chinese Academy of Sciences, Beijing 100190, China
[b] Graduate School of Chinese Academy of Sciences, Beijing 100049, China

ARTICLE INFO

Article history:
Received 14 May 2009
Received in revised form 16 June 2009
Accepted 17 June 2009
Available online 24 June 2009

Keywords:
Gadolinium-doped ceria
Supercritical fluid drying
Sintering
Ceramics

ABSTRACT

Nanocrystalline $Ce_{0.8}Gd_{0.2}O_{1.9}$ (GDC20) powder was synthesized by ammonia co-precipitation combined with supercritical ethanol drying route, followed by characterizations with TG/DSC, XRD, BET, HR-TEM, and FESEM techniques. After calcination at 600 °C, the powder has a high specific surface area of 146.5 $m^2 g^{-1}$ and an average crystal size of ~5 nm without hard-agglomeration. The nano-GDC powder showed excellent sinterability, where by pressureless sintering at 900 °C for 4 h, the relative density of more than 98% and average grain size of 84 nm have been attained, which is attributed to the powder's ultrafine nanocrystal size, weak agglomeration and high homogeneity. Investigations indicate that in the initial sintering stage, grain growth behavior is mainly controlled by volume diffusion mechanism with an activation energy of ~5.4 eV.

1. Introduction

Solid oxide fuel cell (SOFC) is an environmentally friendly energy-transfer equipment with high efficiency. Intermediate-temperature (500–800 °C) solid oxide fuel cells (IT-SOFCs) attract much attention because of their lower fabrication and operation costs compared with the high-temperature ones (above 800 °C). Rare earth-doped ceria is superior to yttria stabilized zirconia (YSZ) as the electrolyte for the IT-SOFCs in respect to the higher oxygen ion conductivity [1–5]. However, one of the main problems concerning the application of the ceria-based electrolyte to IT-SOFCs is their relatively poor sinterability, which makes it difficult for the fabrication of ceria-based SOFCs. It is therefore of great significance to lower the sintering temperature of the ceria-based electrolytes. The addition of trace amounts of transition metal oxides (Co, Mn, Fe, etc.) [6–9] and other alkaline or alkaline–earth metal oxides [10,11] as sintering aids is an effective way to obtain highly densified ceria-based electrolytes at low temperatures. Unfortunately, this usually results in higher electronic conductivity and leads to increased grain-boundary resistance, which plays a negative role for open circuit voltage (OCV) and power output of SOFCs [12].

The alternative solution to the densification problem is to synthesize doped ceria ceramic ultrafine powders, with high specific surface areas and without hard-agglomeration. Nanocrystalline powders exhibit outstanding sinterability because of their huge surface free energies and corresponding fast densification kinetics [13–15]. Moreover, the dense nanocrystalline ceramic electrolyte possesses higher ionic conductivity and better mechanical properties than the micro- or submicro-crystalline one [16,17]. Researches concerning the reduction of the sintering temperature of ceria-based electrolytes focus mainly on gadolinium or samarium-doped ceria (SDC) for the reason that both of them show leading oxygen ion conductivities in the family of ceria solid solutions. Mori and his research group have paid much attention to the sintering of ceria solutions and achieved amazing accomplishments by optimizing synthesis methods of powders. Using a mimic alkoxide method, CeO_2 powders with high sintering activity were obtained and the corresponding ceramic compacts were densified to >99% of the theoretical density after sintering at 1000 °C for 2 h [14]. Furthermore, carbonate and hexamethylenetetramine (HMT)-based co-precipitation routes were employed for preparing samarium or gadolinium-doped ceria (GDC) and nearly fully dense bodies were obtained via pressureless sintering at 1000 °C [15,18]. Recently, the densification temperature was further decreased to 950 °C for the sintering of yttria-doped ceria [19], which was the lowest reported densification temperature for ceria solid solutions up to now. Although many different wet-chemical synthesis methods have been applied to prepare nanosized powders, few reports concentrated on optimizing the sinterability of powders through special drying processes. Our colleague previously reported the low-temperature sintering behavior of nanocrystalline scandia stabilized zirconia (ScSZ) powders prepared via co-precipitation combined with supercritical fluid drying (SCFD) process [20]. The results showed that the compacted pellets achieved above 96% of

* Corresponding author. Tel.: +86 10 62536108; fax: +86 10 62536108.
E-mail address: qszhu@home.ipe.ac.cn (Q. Zhu).

0378-7753/$ – see front matter © 2009 Elsevier B.V. All rights reserved.
doi:10.1016/j.jpowsour.2009.06.058

the theoretical density with an average grain size of ~80 nm at 900 °C for 4 h, inferring that SCFD is an effective strategy for promoting the sinterability of powders.

In this paper, by analogy, we prepared $Ce_{0.8}Gd_{0.2}O_{1.9}$ nanopowders via ammonia co-precipitation combined with the subsequent SCFD method. The crystal structure, the morphology, and the low-temperature sintering behaviors of the powders were investigated, and the sintering mechanism was discussed.

2. Experimental

The synthesis procedure of $Ce_{0.8}Gd_{0.2}O_{1.9}$ powder is similar to the previous work [20]. Briefly, stoichiometric amounts of $Ce(NO_3)_3{\cdot}6H_2O$ and $Gd(NO_3)_3{\cdot}6H_2O$ were dissolved in deionized water to form homogeneous solution with the total metal ion concentration of 0.18 mol L^{-1}. Then, a given quantity of polyethylene glycol (PEG) (analytical-reagent grade) was added into the above-mentioned solution. The pre-prepared 2.5 wt.% ammonium hydroxide was poured into the above-mentioned solution. During this process, the solution was stirred vigorously. Then, mild stirring lasted for about 30 min to insure the completion of the co-precipitation reaction, after which the obtained hydrogel was collected by suction filtering, and washed with deionized water and absolute ethanol sequentially to get rid of the unwanted water. The alcogel was subsequently dispersed in ethanol by an ultrasonator before being transferred into an autoclave. The supercritical fluid drying process was operated at 260 °C for 1–2 h under 8 MPa. After releasing ethanol vapor at 260 °C, the resultant powder was cooled down to room temperature. The as-prepared powders (the powders immediately taken out from the autoclave) were calcined at the selected temperature for 2 h with a heating rate of 5 °C min^{-1} to remove the residual ethanol.

Thermogravimetry/differential scanning calorimetry (TG/DSC, Netzsch STA 449, Germany) was used to investigate the as-prepared powders in flowing air with a heating rate of 10 °C min^{-1}. The crystal phases of the as-prepared and the calcined powders were analyzed using X-ray diffractometry (XRD, X'Pert MPD pro, PANalytical, the Netherlands) with Cu Kα radiation in the range of $2\theta = 20–90°$, and the crystallite size of the calcined powder was estimated from the Scherrer equation [21].

The Brunauer–Emmett–Teller (BET) specific surface area was obtained via N_2 adsorption at 77 K (Autosorb-1, QUANTACHROM, USA) and the measured result was translated into the equivalent particle size according to the following equation:

$$d_B = \frac{6 \times 10^3}{\rho_{th} S_{BET}} \quad (1)$$

where d_B (nm) is the average particle size, S_{BET} is the specific surface area expressed in $m^2\ g^{-1}$, and ρ_{th} is the theoretical density of the solid solution oxide (g cm^{-3}) calculated according to the following equation [22]:

$$\rho_{th} = \left[\frac{4}{N_A a_0^3}\right][(1-x)M_{Ce} + xM_{Gd} + (2-0.5x)M_O] = 7.2327\ \text{g cm}^{-3} \quad (2)$$

where x is 0.2, N_A is the Avogadro constant, M_i is the atomic weight, and a is the lattice parameter of CeO_2.

The morphology and the crystalline size of the calcined powders were investigated by high-resolution transmission electron microscope (HR-TEM, FEI Tecnai F20, the Netherlands). Field-emission scanning electron microscope (FESEM, JSM-6700F, JEOL, Japan) was also used to characterize the morphology and the agglomeration of the as-prepared and calcined powders.

The calcined powder was firstly uniaxially pressed into cylinders under a pressure of about 50 MPa, and then subjected to a cold isostatic press at 200 MPa for 1 min. The resultant green bodies are ~2 mm thick with a diameter of ~10 mm.

Non-isothermal sintering behaviors of the compacted bodies were tested in stagnant air using a dilatometer (L75/1550, LINSEIS, Germany) from room temperature up to 1300 °C with a heating rate of 10 °C min^{-1}. The density of the measured compact, ρ, at any temperature, was calculated via the following equation:

$$\rho = \frac{\rho_0}{(1 + \Delta L/L_0)^3} \quad (3)$$

where ρ_0 is the density of a green compact determined from its weight and geometric dimensions, L_0 is the original sample length, and, $\Delta L = L - L_0$, where L is the instantaneous sample length. Isothermal sintering was carried out in a muffle furnace at selected temperatures with a heating rate of 2 °C min^{-1} and a soaking time of 4 h.

The microstructures of the sintered bodies were investigated via FESEM. Average grain sizes of the as-sintered electrolyte were determined by the linear intercept method from at least 100 randomly selected grains. The densities of the densified ceramics were measured by the Archimedes method with deionized water as an intrusion medium and three measurements were repeated to obtain the average values of the results.

3. Results

Thermal decomposition behavior of the as-prepared GDC20 powder is shown in Fig. 1. Continuous weight loss of the powder in the testing temperature is revealed, which can be roughly divided into two stages without obvious boundary. The first stage, with the exothermic peak at ~210 °C, is assigned to the decomposition of the residual hydroxide. The exothermic peak occurring at ~250 °C on the DSC curve is attributed to the desorption and burn-off of the ethanol adsorbed on the surface of the powder. From room temperature to 400 °C, there is a total weight loss of ~7.4%. According to Fig. 1, in order to absolutely remove the residual hydroxide and ethanol, 600 °C was selected to be the calcination temperature of the as-synthesized powder.

The crystallite structures of powders were analyzed by X-ray diffraction measurements. Both of the as-prepared powder and the powder calcined at 600 °C for 2 h display the reflection peaks of the fluorite-like CeO_2 (Fig. 2). No Gd_2O_3 crystalline phase was observed from the XRD pattern, which suggests that Gd_2O_3 has totally dissolved into the lattice of CeO_2, forming a single-phase solid solution. The crystalline phase of the powder was well-developed after calcination, which was confirmed through the sharper XRD peaks of the calcined powder.

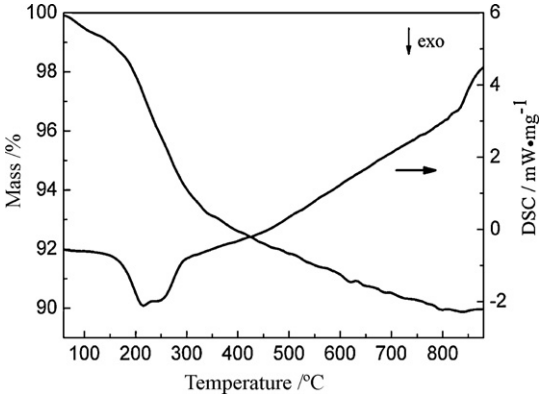

Fig. 1. TG/DSC curves of the as-prepared GDC20 powder in flowing air at a heating rate of 10 °C min^{-1}.

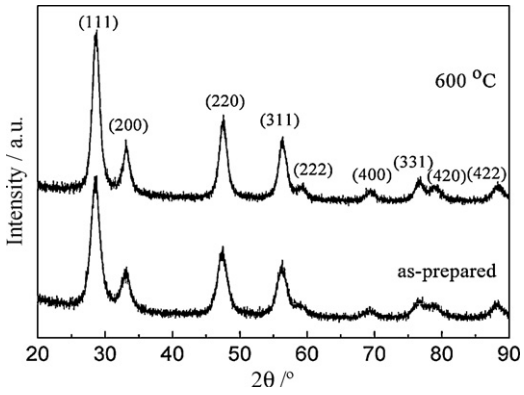

Fig. 2. XRD patterns of the as-prepared GDC20 powders and the powders calcined at 600 °C for 2 h.

The equivalent particle size of the as-calcined powder was obtained indirectly through XRD and the specific surface area measurement. The crystallite size is calculated to be 7.7 nm by the X-ray line broadening technique performed on the (1 1 1) diffraction peak. The BET specific surface area is 146.5 $m^2\ g^{-1}$, and the corresponding equivalent particle size is ~5.6 nm by assuming a spherical particle shape. The crystalline size has also been directly observed using a high-resolution transmission electron microscope (TEM). As shown in Fig. 3, the calcined nanoparticles possess approximately spherical shape. Moreover, the size distribution of the particles is very uniform and the average crystallite size is ~5 nm, which agrees well with the results determined by XRD and BET measurements, indicating a well-defined dispersing state without significant hard-agglomeration.

Typical morphologies and agglomeration states of the nanopowder with and without the heat treatment are compared in Fig. 4, from which it can be seen that the secondary particles are ~30 nm, consisting of the primary ultrafine particles smaller than 10 nm. The SEM observation results are in good accord with the results obtained by XRD, BET and TEM, indicating that the investigations were performed on the same entities.

The non-isothermal sintering behavior of the green body was recorded via the dilatometer under a constant heating rate of 10 °C min^{-1} and is shown in Fig. 5. With the green density of 49.3%,

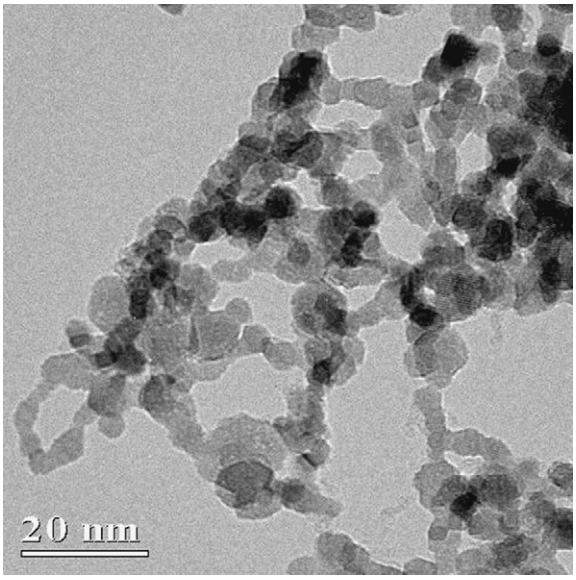

Fig. 3. The HR-TEM image of the GDC20 powders calcined at 600 °C for 2 h.

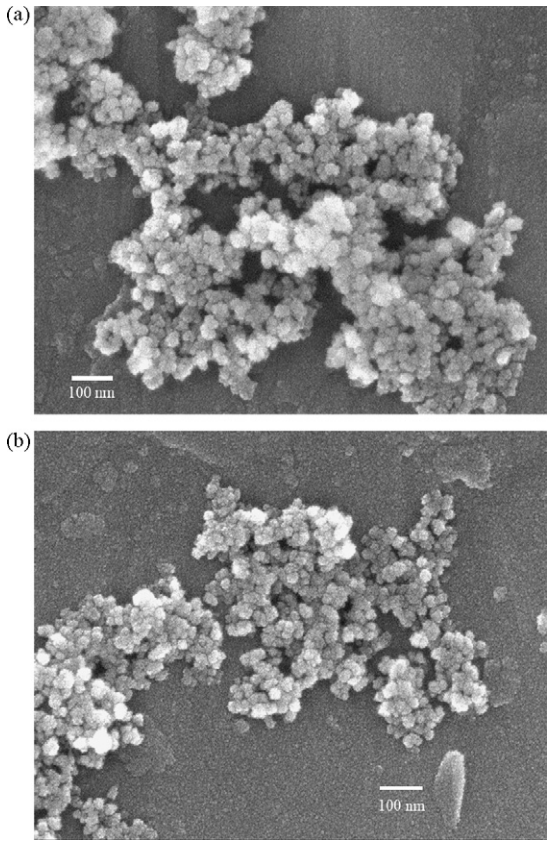

Fig. 4. FESEM micrographs of the GDC20 powders (a) as-prepared, and (b) after calcination at 600 °C for 2 h.

the relative density of the cylinder achieves up to ~99% when the heating temperature climbs up to 1050 °C, where can be roughly considered as the dead end of the sintering actions of the powders. It is also shown in Fig. 5 that the peak of the densification rate curve is not very sharp but accompanied with wide shoulders, indicating that the densification rate of the object turns to be relatively slow during the final stage of sintering considering the heat treatment at 600 °C. The maximum shrinkage rate locates at 716 °C, a record of extremely low temperature among the reported data, demonstrating the excellent sinterability of the synthesized nanopowder.

Isothermal sintering experiments of the green bodies were executed in a muffle furnace at 800–1100 °C for 4 h in still air at a heating rate of 2 °C min^{-1}. The microstructures and morphol-

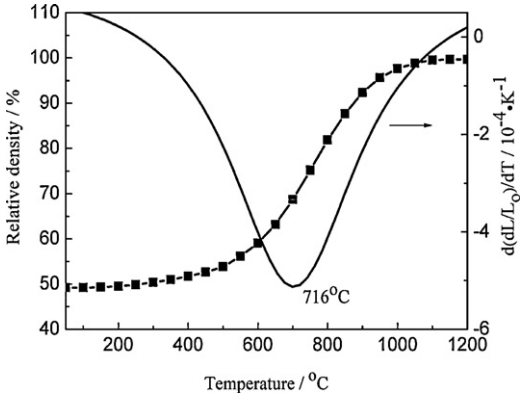

Fig. 5. Densification behaviors of the GDC20 compact with the powders calcined at 600 °C for 2 h, recorded via dilatometry at a heating rate of 10 °C min^{-1} in static air.

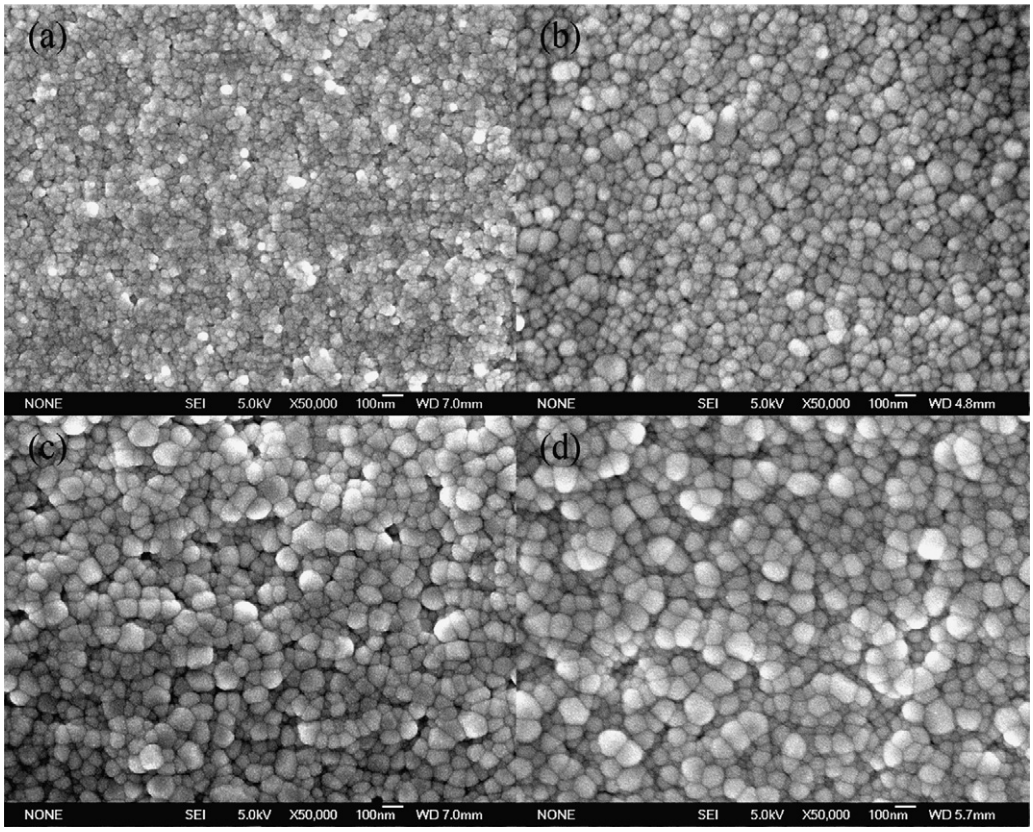

Fig. 6. FESEM micrographs of the sintered GDC20 ceramics sintered at (a) 800 °C, (b) 900 °C, (c) 1000 °C, and (d) 1100 °C for 4 h in still air.

ogy of the sintered samples are shown in Fig. 6. After sintering at 800 °C for 4 h, the compact has been densified to ~95% of the theoretical density, and a lot of fine pores or lacunas still exist. Fortunately, the rate of densification of the system is very fast and the grains simultaneously grow rapidly at this stage, inferring that the ceramics can be densified fully at a certain low temperature not much higher than 800 °C. And, indeed, in Fig. 6(b), when the sintering temperature increases to 900 °C, the relative density of the body exceeds 98% of the theoretical value and the average grain size is ~84 nm. In addition, grains appear to have strong facets and the grain boundaries become very clear and straight, both of which are the typical features of the ceramics in the final sintering stage. Fine pores or lacunas are eliminated gradually and densification is further improved with the increase of sintering temperature. Average grain sizes of the compacts isothermally sintered at various temperatures, shown in Fig. 7, are obtained through the linear intercept technique after converting the measured values to true grain sizes by multiplying with a factor of 1.56 [23]. According to the above observation, the average primary particle size of the green compact is ~5 nm, while it increases by a factor of 7 to ~38 nm after sintering at 800 °C for 4 h, indicating a fast coarsening rate of the particles during this stage. The average particle/grain size increases a little more than two times from 800 to 900 °C. In the subsequent sintering stage from 900 to 1100 °C, the growth of the grains proceeds comparatively slowly: the average grain sizes are 101 nm for 1000 °C, and 118 nm for 1100 °C. The relative densities of the sintered bodies to the theoretical value, measured by the Archimedes method, as a function of sintering temperature are plotted in Fig. 8. From 800 to 900 °C, both of the rates of coarsening and densification are relatively high. During this process, the particles/grains have no enough free spaces to relocate or rearrange, and thus the rapid grain-boundary migration sweeps across the smaller particles, making the larger

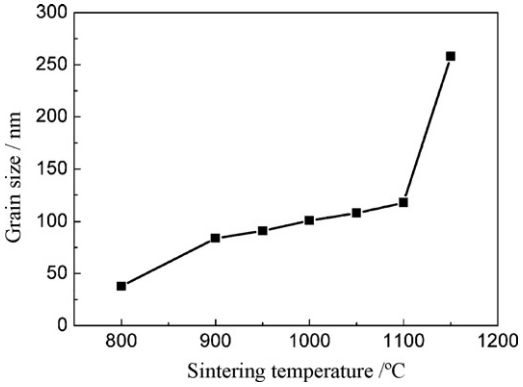

Fig. 7. Average grain sizes of the sintered GDC20 ceramics, as a function of sintering temperature. The soaking time at each temperature is 4 h.

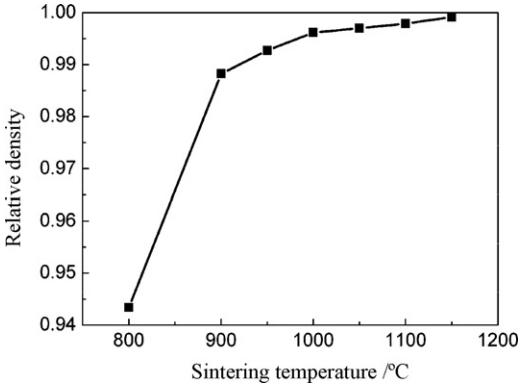

Fig. 8. Relative density values of the GDC20 compacts, as a function of the sintering temperature. The residence time at each temperature is 4 h.

particles swallow the smaller ones, which results in the coarsening of grains and the simultaneous elimination of intergranular fine pores [24]. With the temperature elevated to 1100 °C, both of the rates of grains growth and ceramics densification slow down, which may be attributed to the higher activation energy of grain-boundary movement and the lower driving force for sintering at the final stage. When the ceramics reaches nearly full densification, the increase of sintering temperature solely brings in the growth of grains, thus the average grain size quickly climbs up to 258 nm.

4. Discussion

Sintering is a process that the surface energy of the system decreases gradually. The original solid-gas interfaces are eliminated, and meanwhile, the new solid–solid boundaries form. It is well known that nanosized powders exhibit amazing sinterability due to their high surface energy, so lots of researches concentrated on improving powder sinterability through particle size. Co-precipitation is a commonly used route for synthesizing homogenous nanopowders. In order to acquire powders of good sintering activity, washing with ethanol is necessarily recommended, and subsequent drying in flowing N_2 or air is also helpful [14]. In fact, drying the hydrogel/alcogel under a supercritical condition is superior to the both. Theoretically, under a SCFD condition, the surface tension is zero, and powders disperse to the highest extent, leading to the lowest agglomeration of resultant powders [20,25]. For ethanol, SCFD process runs under a harsh condition with high temperature and high pressure (260 °C under 8 MPa in this experiment), so the crystallization of the raw aerogel accomplishes almost completely (see Fig. 2), especially for the doped ceria whose crystallization can be realized in atmosphere. Based on this fact, the as-prepared powders can be compacted directly for next investigations. However, according to the TG/DSC curves, the residual hydroxide and the adsorbed ethanol with several percent is still contained in the fresh powders, and direct utilization without calcination will hinder the subsequent densification process due to the decomposed gases. Admittedly, calcination promotes grain growth, which cuts down powders' sintering activity, but, on the other hand, it increases green densities of compacts, which is beneficial for the low-temperature sintering. However, in our experiment, they are balanced and it was found that particles after calcination at 600 °C for 2 h remain loose conglomeration and the average grain size is only ~5 nm. The particle together with the weak agglomerate state endues the excellent sinterability of the GDC20 powder that could be densified at a temperature at least 50 °C lower than the reported value before [19].

Herring's scaling law assuming that particles remain geometrically identical during sintering besides a change in scale was widely applied to study the quantitative influence of grain/crystal size on densification behaviors of ceramics. The linear shrinkage rate is expressed as the following equation if grain-boundary diffusion or volume diffusion were the dominating densification mechanism [26]:

$$-\frac{\mathrm{d}L}{L\,\mathrm{d}t} = \frac{\gamma\Omega}{kT}\left(\frac{\Gamma D_0}{G^n}\exp\left(-\frac{Q}{kT}\right)\right) \tag{4}$$

where L is the actual sample length, t is the time, γ is the surface energy, Ω is the atomic volume, k is the Boltzmann constant, T is the current temperature, G is the actual grain size, and Q is the activation energy. Γ, D_0, and n are specific to the dominant diffusion mechanism. For grain-boundary diffusion, $n = 4$; for volume diffusion, $n = 3$. The shrinkage rate as a function of temperature can be obtained by transforming Eq. (4) into:

$$\frac{\mathrm{d}L}{\mathrm{d}T} = -\frac{AL}{TG^n}\exp\left(-\frac{Q}{kT}\right) \tag{5}$$

where

$$A = \frac{\gamma\Omega\Gamma D_0}{k\,\mathrm{d}T/\mathrm{d}t}$$

Eq. (5) describes the relationship between the peak position and height of the maximum densification rate and the activation energy. Provided that all factors in A are constant and also grain growth information is known in detail during sintering process, the activation energy Q of the densification can be calculated by differentiating Eq. (5) and equating the result to zero. Then, by rearranging the result, a clearer dependence of Q on the maximum shrinkage rate is obtained:

$$\frac{Q}{k} = T_{\max} - \frac{T_{\max}^2}{L_{\max}}\left(\frac{\mathrm{d}L}{\mathrm{d}T}\right)_{\max} - \frac{T_{\max}^2}{G_{\max}^n}\left(\frac{\mathrm{d}G^{-n}}{\mathrm{d}T}\right)_{\max} \tag{6}$$

Grain coarsening rate at the first region is assumed to be slow, and the third term on the right-hand side can be treated as zero. Based on the data in this experiment, the activation energy of densification, Q, was calculated to be 0.143 eV, indicating a huge discrepancy from the reported values of 4–7 eV [24,26,27]. Therefore, the practical grain growth rate is quite fast, accompanying with effectively quick adjusting of grains' locations, leading to obvious shrinkage in macroscopic scale.

Efforts have been done to anatomize the densification behaviors of ceramics during the initial-stage sintering process. Under a constant heating rate condition, the activation energy Q can also be calculated through the following equation [6]:

$$\ln\left[\frac{\Delta L/L_0}{T}\right] = -\frac{Q}{(m+1)R}\frac{1}{T} + \ln B \tag{7}$$

Here, L_0 is the original length of the sample, B is a constant referring to the material parameters and the sintering mechanisms, and m is a constant only depending on the specific densification mechanism. For the volume diffusion, $m = 1$; for the grain-boundary diffusion mechanism, $m = 2$. The other symbols have the same meanings as in Eq. (4). Fig. 9 illustrates the linear part of Eq. (7) based on our experimental results, and the fitting slope of the curve was −0.32538 calculated through the least squares method. Sintering of nanocrystalline CeO_2 and SDC powders are considered to be controlled by the grain-boundary diffusion mechanism [28], and if it is realistic here, the activation energy Q calculated according to Eq. (7) is 8.1 eV, much higher than the reported ones. When $m = 1$, Q is 5.4 eV, a reasonable value indicating the initial densification process of our

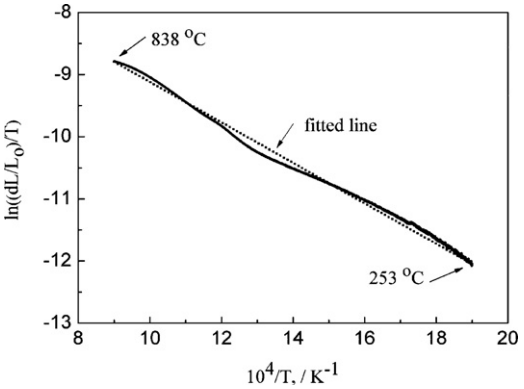

Fig. 9. Relationship of $\ln[(\Delta L/L_0)/T]$ versus the inverse of temperature for GDC20 sintered at a heating rate of 10 °C min^{-1} in static air.

GDC20 nanopowders is controlled by the volume diffusion mechanism. Then the densification rate of our nanoparticle (~5 nm) is more than one order of magnitude greater than that of the reported nanopowder (~15 nm), whose full densification can be achieved at 1000 °C for 4 h [15].

5. Conclusions

The ammonia co-precipitation combined with supercritical ethanol drying route has been employed to synthesize $Ce_{0.8}Gd_{0.2}O_{1.9}$ powder with nitrates as the starting salts and PEG as the dispersant. The powder was characterized by TG/DSC, XRD, BET-N_2 adsorption, HR-TEM and FESEM techniques, and the densification behavior was investigated by non-isothermal sintering via dilatometry and isothermal sintering at a constant heating rate. The powder calcined at 600 °C for 2 h has a high specific surface area of 146.5 $m^2\ g^{-1}$ with an average crystal size of ~5 nm. The as-calcined powder showed excellent sinterability, where green bodies can be sintered to over 98% of the theoretical density at 900 °C for 4 h. The extraordinary densification activity of GDC20 powder in the present work is attributed to the ultrafine nanocrystal size and its weak agglomeration. In the initial sintering region, grain growth behavior is mainly controlled by the volume diffusion mechanism with the activation energy of ~5.4 eV.

Acknowledgement

Financial support from the National Natural Science Foundation of China (No. 50730002 and No. 20776143) is acknowledged.

References

[1] N.Q. Minh, J. Am. Ceram. Soc. 76 (1993) 563.
[2] B. Riley, J. Power Sources 29 (1990) 223.
[3] H. Inaba, H. Tagawa, Solid State Ionics 83 (1996) 1.
[4] M. Godickemeier, L.J. Gauckler, J. Electrochem. Soc. 145 (1998) 414.
[5] B.C.H. Steele, Solid State Ionics 129 (2000) 95.
[6] T.S. Zhang, P. Hing, H. Huang, J. Kilner, Mater. Sci. Eng. B 83 (2001) 235.
[7] T.S. Zhang, P. Hing, H. Huang, J. Kilner, J. Eur. Ceram. Soc. 22 (2002) 27.
[8] C. Kleinlogel, L.J. Gauckler, Solid State Ionics 135 (2000) 567.
[9] E. Jud, L.J. Gauckler, J. Electroceram. 14 (2005) 247.
[10] J.D. Nicholas, L.C.D. Jonghe, Solid State Ionics 178 (2007) 1187.
[11] V. Gil, J. Tartaj, C. Moure, P. Duran, Ceram. Int. 33 (2007) 471.
[12] D.P. Fagg, V.V. Kharton, J.R. Frade, J. Electroceram. 9 (2002) 199.
[13] C. Herring, J. Appl. Phys. 21 (1950) 301.
[14] J.G. Li, T. Ikegami, J.H. Lee, T. Mori, Acta Mater. 49 (2001) 419.
[15] J.G. Li, T. Ikegami, T. Mori, Acta Mater. 52 (2004) 2221.
[16] P. Mondal, A. Klein, W. Jaegermann, H. Hahn, Solid State Ionics 118 (1999) 331.
[17] C. Tian, S.W. Chan, Solid State Ionics 134 (2000) 89.
[18] J.G. Li, Y.R. Wang, T. Ikegami, T. Mori, T. Ishigaki, Mater. Sci. Eng. B 121 (2005) 54.
[19] J.G. Li, Y.R. Wang, T. Ikegami, T. Ishigaki, Solid State Ionics 179 (2008) 951.
[20] Z. Lei, Q.S. Zhu, Solid State Ionics 176 (2005) 2791.
[21] H.P. Klug, L.E. Alexander, X-ray Diffraction Procedures for Polycrystalline and Amorphous Materials, John Wiley and Sons, New York, 1974, p. 618.
[22] A.I.Y. Tok, L.H. Luo, F.Y.C. Boey, Mater. Sci. Eng. A 383 (2004) 229.
[23] M.I. Menddson, J. Am. Ceram. Soc. 52 (8) (1968) 443.
[24] P.L. Chen, I.W. Chen, J. Am. Ceram. Soc. 80 (3) (1997) 637.
[25] M.A. Thundathil, W. Lai, L. Noailles, B.S. Dunn, S.M. Haile, J. Am. Ceram. Soc. 87 (8) (2004) 1442.
[26] E. Jud, C.B. Huwiler, L.J. Gauckler, J. Am. Ceram. Soc. 88 (11) (2005) 3013.
[27] R.Q. Yan, F.F. Chu, Q.L. Ma, X.Q. Liu, G.Y. Meng, Mater. Lett. 60 (2006) 3605.
[28] T. Ikegami, Key Eng. Mater. 247 (2003) 51.